Scanning Tunneling Microscopy Study of the Structural Phase Transformation in Manganese Nitride: θ-MnN $\rightarrow$ η-Mn_3N_2

Rong Yang, Muhammad B. Haider, Haiqiang Yang*, Hamad Al-Brithen, Arthur R. Smith†

Condensed Matter and Surface Science Program, Department of Physics and Astronomy, Ohio University, Athens, OH 45701

Abstract

The phase transformation of a (001)-oriented θ-MnN thin film grown by molecular beam epitaxy to η-Mn_3N_2 has been investigated using a combination of diffraction analysis and real-space surface analysis by scanning tunneling microscopy. The θ-MnN thin film is prepared by growth at 450°C; it is then annealed at 550°C. It is found that the phase transformation results in 3 different orientations of the η-Mn_3N_2 phase within the annealed film. The phase transformation is attributed to diffusion and loss of N atoms and ordering of the N-vacancies into parallel sheets. A schematic model of the annealed film structure is presented.

PACS: 68.37Ef, 68.35Bs, 68.55Jk, 75.50Ee, 81.10 Bk

---

*Present address: Department of Physics ,Texas A & M University, College Station, TX 77840

†Corresponding author, Email: smitha2@ohio.edu; Fax: 1-740-593-0433

I. INTRODUCTION

Transition metal nitrides have drawn much attention due to their attractive physical properties, including structural, optical, electronic, and magnetic properties, and their potential applications in various fields, including optical coatings, magnetic recording and sensing.[1–4] Recently, Mn doping of GaN[5–8] has been studied because of the possibility of forming a diluted magnetic nitride semiconductor (DMNS) with a high Curie temperature. In fact, manganese nitride (Mn_xN_y) by itself is attractive as a magnetic material having unique and variable magnetic properties.[9–17] The magnetic properties, which could potentially allow for the formation of magnetic/non-magnetic nitride semiconductor multilayers or ferromagnetic(FM)/antiferromagnetic(aFM) multilayers, depend on the Mn:N composition ratio which affects the phase. Several different phases are known in manganese nitride including θ (MnN), η (Mn_3N_2), ζ (Mn_5N_2, Mn_2N, and $Mn_2N_{0.86}$) and ϵ (Mn_4N) . Both θ-MnN and η-Mn_3N_2 phases are antiferromagnetic with reported Néel temperatures of 650K[10,11] and 925K[10], respectively. The Mn_4N phase is ferrimagnetic with a reported Curie temperature of 738K.[12] Because of these phase-dependent magnetic properties, it is of great interest to explore methods of controlling the phase and orientation of manganese nitride layers.

Recently, Yang *et al.* reported how to control the phase and orientation of manganese nitride layers grown on MgO(001) substrates by varying the Mn/N flux ratio J_{Mn}/J_N and also by varying the substrate temperature.[15] It has been shown that θ, η, and ε phases can each be grown at a single growth temperature by choosing the Mn:N flux ratio; also, the crystalline orientation of the η-phase depends on the flux ratio.

Suzuki *et al.* showed through a study of manganese nitride powders, that these phases have different ranges of thermal stability, where the less N-rich phases were stable at higher temperatures.[10] It is therefore interesting to explore the temperature stability of our MBE-grown, and highly oriented, manganese nitride films. In this work, we investigate the phase transition from $\theta \rightarrow \eta$ of our highly-oriented MBE grown thin film by means of annealing; we show how the transformation occurs at the atomic scale using scanning tunneling microscopy

(STM). Lastly, a schematic model of the annealed film surface is presented.

II. EXPERIMENT

The growth experiments are performed in a custom-designed ultra-high vacuum (UHV) system consisting of an all-nitride MBE chamber coupled to a surface analysis chamber. The MBE system includes a solid source effusion cell for Mn and a RF plasma source for N. The experimental procedure is, briefly, to grow θ-phase MnN, anneal the film to higher temperature, then cool the film to room temperature for examination by *in-situ* UHV STM. After removal from the analysis chamber, the samples are analyzed using x-ray diffraction (XRD) with Cu K_α x-rays.

The detailed procedure is as follows: after being heated up to 950 °C for 30 minutes with the nitrogen plasma turned on, the MgO substrate temperature is lowered to 450 °C. Then the MnN layer is grown at 450 °C with nitrogen flow rate $\sim$ 1.1 sccm (growth chamber pressure is 1.1×10^{-5} Torr) with the RF power set at 500 W. The θ-phase is grown with Mn flux = 7.3×10^{13}/cm^{2}s. The MnN film thickness for this study was $\sim$ 400 Å. The growth condition is monitored using reflection high energy electron diffraction (RHEED). Growth stops by closing the Mn shutter; then the annealing begins by increasing the sample temperature to 550 °C, still with N-plasma on. As a final step, after 15 minutes of annealing, the Mn shutter is opened for 40 seconds to refresh the surface.

III. RESULTS AND DISCUSSION

A. Orientations of Manganese Nitride Phases Grown by MBE on MgO(001)

Shown in Fig.1(a-c) are schematic side-view models for the θ-MnN and η-Mn_3N_2 phases/orientations of manganese nitride grown on MgO(001) as a function of Mn:N flux ratio. These models were derived from growth experiments performed as a function of Mn:N flux ratio and reported previously.[15] From these models, the similarities between the

phases/orientations can be seen. The θ-MnN and η-Mn_3N_2 are both fct. Both have octahedral bonding. This allows one to view them as variations of a simple structure with N vacancies. One can see that the θ phase consists of a fct Mn sublattice which is fully occupied together with a fct N sublattice which is almost fully occupied. The η-Mn_3N_2-phase can be viewed similarly as consisting of a fully occupied Mn fct sublattice together with a N fct sublattice which is 2/3 occupied in a repeating layered structure. The two orientations of η-phase which can be prepared under different Mn:N flux ratio are denoted $\eta_\perp$and $\eta_\parallel$.

B. RHEED and XRD Analysis of θ-MnN $\rightarrow$ η-Mn_3N_2 Phase Transformation

1. RHEED and XRD of As-Grown Sample: θ-MnN with (001) Orientation

To determine *in-plane* lattice parameters, RHEED is performed, as shown in Fig. 2. The patterns were acquired with the electron beam along the $[100]_{MgO}$ direction. The RHEED patterns shown in Figs. 2(a,b) present the stages of the growth of θ-MnN (001). Fig. 2(a) is the RHEED pattern of MgO(001) at 450 °C, which shows a well-oriented crystalline starting surface and corresponding to a lattice constant of $a_{MgO} = 4.213$ Å.[18] The RHEED pattern of the as-grown θ-MnN surface [shown in Fig. 2(b)] is slightly streakier than that of MgO and shows almost no change in the streak spacing, giving an *in-plane* lattice parameter of 4.21 Å, which is slightly smaller than but very close to the reported value $a_{MnN} = 4.22$ Å by Yang *et al.* for thicker films.[15]. Thus the RHEED indicates that the sample has the *a* lattice directions *in-plane*.

To determine *out-of-plane* lattice parameters, XRD is performed at room temperature, as shown in Fig. 3. The spectra are plotted in semi-log scale to amplify small peaks. While our x-rays include both $K\alpha 1$ and $K\alpha 2$, an average $K\alpha$ wavelength of $\lambda = 1.542$ Å is used to calculate the *d* spacings. As shown in Fig. 3(a), for θ-MnN as-grown, XRD shows two significant peaks. The first peak at 42.94° is 002 of MgO; the second peak at 43.99° is 002 of θ-MnN,[15] which corresponds to a lattice constant of 4.12 Å, in good agreement with the

reported value of c for θ-MnN.[11,15] In addition to the main peaks seen in Fig. 3(a), another tiny peak at 47.06° corresponding to the 002 peak of ε-Mn_4N also appears; however, the intensity of this peak is much smaller than the intensity of the θ-MnN 002 peak, showing that the as-grown film is at least 99% MnN phase having (001) orientation. The (001) orientation is partly attributed to the excellent lattice match between a_{MnN} and a_{MgO}.

2. RHEED and XRD of Annealed Sample: η-Mn_3N_2 with Mixed Orientation

Figure 2(c) shows the RHEED pattern of the sample after annealing at 550 °C under N plasma flux for 15 minutes. The RHEED pattern is nearly identical to that of the as-grown sample in Fig. 2(b). The very small change of streak spacing ($\leq$0.5%) shows that the *in-plane* lattice constant is still very close to 4.21 Å.

Figure 2(d) is the RHEED pattern of the sample after annealing and depositing a very small amount of Mn, followed by cooling down to room temperature. Although the primary streak spacing is hardly changed from the annealed-only sample, the RHEED pattern shows additional features: namely, weak $\frac{1}{3}$-order fractional streaks along $[100]_{MgO}$. Such $\frac{1}{3}$-order streaks indicate η-phase Mn_3N_2 with c-axis parallel to the surface plane. The $\frac{1}{3}$-order streaks give an *in-plane* spacing of 12.22 Å, which agrees well with c of η-phase (12.14 Å).

For the sample after annealing and Mn deposition, we observe a different set of peaks in the XRD spectrum, as shown in Fig. 3(b). The first main peak is again 002 of MgO at 42.94°; the second main peak occurs at 44.81°, which is 006 of $\eta_\perp$-Mn_3N_2, and corresponds to a lattice parameter of 12.14Å, which is equal to c of η-Mn_3N_2. The third main peak occurs at 29.45°, which is 004 of $\eta_\perp$. So, the annealed film clearly contains $\eta_\perp$ orientation, and there is no longer any sign of the θ-MnN phase in the XRD spectrum. However, the annealed film can also contain $\eta_\parallel$ orientation since the $\eta_\parallel$ 020 peak coincides with the MgO 002 peak at 42.94°.

Combining the RHEED and XRD results together, we find that after annealing and Mn deposition, the thin film sample of (001)-oriented θ-MnN has transformed to a combination

of (001)- and (010)-oriented η-Mn_3N_2 (referred to as $\eta_\perp$ and $\eta_\parallel$, respectively). We note that our growth of θ-MnN at 450°C and annealing to η-Mn_3N_2 at 550°C is consistent with the phase transformation temperature of 480°C from θ-MnN to η-Mn_3N_2 for bulk MnN powders obtained by Suzuki *et al.*[10]

C. Atomic-Scale Analysis of Phase Transformation by STM

1. STM of As-Grown Surface: θ-MnN with (001) Orientation

To examine these surfaces with atomic-scale resolution, *in-situ* STM has been performed. Shown in Fig. 4 are STM images of the θ-MnN as-grown sample surface. Fig. 4(a) shows a large image of size 900 Å × 900 Å. The growth surface shows large terraces with steps. Large mounds define the surface morphology. Fig. 4(b) shows a medium-size image of 200 Å × 200Å, which consists of terraces separated by steps of height $\sim$ 2.1Å, consistent with $c/2$ of θ-MnN. This image shows that the θ-MnN (001) growth surface has an interesting structure, with evidence of local nanoscale variations which may be due to either N-vacancies or to excess Mn adatoms. Still, the 1×1 atomic-scale structure of the surface can be seen in the zoom-in image of 25Å × 25Å in Fig. 4(c), which corresponds to the small box region in Fig. 4(b). The atomic rows are along [110]. Since θ-MnN is a metal and moreover since the local density of states for Mn atoms is much larger than that for N atoms near the Fermi level,[14] STM images of this surface are expected to show the Mn atoms. Comparing with the ideal 1×1 surface model shown in Fig. 4(d), the STM image of Fig. 4(c) is in good agreement with the Mn sublattice.

2. STM of Annealed Surface: η-Mn_3N_2 with Mixed Orientation

Shown in Fig. 5 are STM images of the annealed and refreshed sample surface. The morphology of the surface is clearly very different compared to the as-grown sample. Fig. 5(a) is a large image of 900Å × 900Å. We find the surface is very smooth with well-defined

step edges. In fact, the annealed surface shows much larger terraces than the as-grown surface. Fig. 5(b) is a 150Å × 150Å image. It consists of featureless areas, some pit-like areas, and some regions of row structures. The featureless regions will be shown (below) to correspond to domains of $\eta_\perp$ orientation. The pit-like regions are attributed to effects of the annealing in which atoms are dislodged from their lattice sites at the surface. Finally, the row structures have a spacing of $\sim$ 6Å. This spacing is in agreement with the spacing between (001) Mn planes of $\eta_\parallel$ which are 3 atomic layers apart. This STM data shows that the weak $\frac{1}{3}$-order fractional streaks seen in the RHEED image of Fig. 2(d) arise from local surface regions having 3× ordering.

Zoom-in STM images of the annealed and refreshed sample surface are shown in Fig. 6(a-c). Two types of areas are seen, one having 1× structure and the other having 3× structure. The 1×1 structure is clearly resolved in Fig. 6(a) and is also seen in parts of Figs. 6(b,c); this evidently corresponds to the η-Mn_3N_2 domain region having the $\eta_\perp$ orientation; the surface area is thus 1×1. Areas in Figs. 6(b,c) showing the 3× row structures(inside dotted loop), on the other hand, correspond to regions having $\eta_\parallel$ orientation. These superstructure rows are along [100] directions and have spacing $\sim$ 6 Å = 3× the primitive atomic spacing which equals $\frac{c}{2}$ of η-Mn_3N_2 (note: the relaxed value of $\frac{c}{2} = 6.07$ Å).[16] It can be seen that the row direction for the 1×1 region ([110]) is at 45° with respect to the row direction of the 3× region ([100]). For comparison with the $\eta_\parallel$ domain regions seen in Figs 6(b,c), shown in Fig. 6(d) is an STM image of as-grown $\eta_\parallel$-Mn_3N_2 (010) in which the 3× row structure makes up the entire surface. It is important to note that the 3× ordering at the surface corresponds directly to the bulk 3× ordering.

D. Interpretation of Annealing Results and Model

The interpretation of the STM data presented in Figs. 4-6 is that prior to annealing, the sample is θ-MnN (001) having a surface with 1×1 structure. After annealing, the film is transformed into η-Mn_3N_2 having domains with all 3 possible orientations of the

c-axis: 1 perpendicular to the surface plane ($\eta_\perp$) and 2 in the surface plane ($\eta_\parallel$). It is somewhat surprising that the $\eta_\parallel$-orientation is produced by annealing since the *in-plane* lattice parameter of the $\eta_\perp$-orientation (4.21 Å) agrees to within 0.24% with the *in-plane* lattice parameter (4.22 Å) of the θ-phase (001)-oriented starting film. Whereas, the $\eta_\parallel$-orientation has 2 relevant *in-plane* lattice parameters: $a = 4.21$ Å and $c/3 = 4.04$ Å. Thus one might expect the (001)-oriented θ-MnN film to transform completely to $\eta_\perp$-orientation since it is the best "fit."

We note, however, that the $3\times$ lines did not really appear until after depositing Mn. This could imply that the $\eta_\parallel$-orientation was grown "on top of" the $\eta_\perp$-orientation. However, in previous experiments, we attempted to grow $\eta_\parallel$ phase as a second layer on top of a first layer of $\eta_\perp$ phase but without success. Therefore, the previous implication is unlikely. The correct interpretation is instead the following. During the annealing, the plasma source was kept on. Exposure to N plasma has been found in previous experiments to result in local disordering of the $\eta_\parallel$ (010) surface. Whereas, subsequent Mn deposition has been found to increase the intensity of the $3\times$ ordering seen in RHEED.[19] This is most likely what occured during the Mn deposition step in this annealing and deposition experiment. It means that in fact, domain regions having $\eta_\parallel$ orientation were created during the annealing but hidden in RHEED due to the N plasma exposure and then revealed by the subsequent Mn deposition.

Fig.7 shows a schematic model of the annealed surface with two different η-Mn_3N_2 orientations. Fig. 7(a) is the top-view model. The model is formed by starting with the θ-MnN (001) surface model and then allowing part of the area to transform to $\eta_\perp$ (with no change of symmetry in the top MnN layer) and part to transform to $\eta_\parallel$. The area corresponding to $\eta_\perp$ (001) has Mn atoms arranged in rows parallel to [110] and [$\bar{1}$10], as shown also in STM image of Fig. 6(a). Within the $\eta_\parallel$ region, N atoms are removed along lines parallel to [010] of $\eta_\perp$ which results in the $3\times$ row structures of $\eta_\parallel$. Consistent with the STM images, those $\eta_\parallel$ $3\times$ rows along [100] are thus at 45° with respect to the $\eta_\perp$ Mn atom rows along [110] and [$\bar{1}$10].

The side view model of the annealed surface is shown in Fig. 7(b). It shows two different

orientations of η-Mn_3N_2 phases with respect to the growth surface. In [001] direction, every third layer of N atoms parallel to the growth surface is missing, resulting in an $\eta_\perp$ domain. As for the $\eta_\parallel$ domain, the c planes are perpendicular to the growth surface.

IV. CONCLUSIONS

In conclusion, the phase transformation from θ-MnN to η-Mn_3N_2 by annealing within a thin manganese nitride film grown by MBE on MgO(001) has been investigated. Both RHEED and XRD confirm that after annealing the θ-MnN thin film at 550°C, it transforms to η-Mn_3N_2. Moreover, the annealed film contains domains of η-Mn_3N_2 having the c-axis in 3 different directions. *In-situ* room temperature STM clearly reveals the 3 types of domains: 2 with the c-axis *in-plane* and 1 with the c-axis *out-of-plane*. The results show that the thin and highly-oriented manganese nitride films undergo phase transformation at temperatures consistent with previous measurements on bulk powders.[10]

V. ACKNOWLEDGEMENTS

This work is supported by the National Science Foundation under grants No. 9983816 and No. 0304314.

REFERENCES

[1] T. D. Moustakas, R. J. Molnar, and J. P. Dismukes, Electrochem. Soc. Proceedings **96-11**, 197 (1996).

[2] D. Gall, I. Petrov. P. Desjardins, and J. E. Greene, J. Appl. Phys. **86**, 5524 (1999).

[3] A. R. Smith, H. A. H. Al-Brithen, D. C. Ingram, and D. Gall, J. Appl. Phys. **90**, 1809 (2001).

[4] S Yang, D.B. Lewis, I. Wadsworth, J. Cawley, J.S. Brooks, and W.D. Munz, Surf. and Coat. Technol. **131**, 228 (2000); K. Inumaru, T. Ohara, and S. Yamanaka, Appl. Surf. Sci. **158**, 375 (2000).

[5] H. Ohno, Science **281**, 951 (1998).

[6] Muhammad B Haider, Costel Constantin, Hamad Al-Brithen, Haiqiang Yang, Eugen Trifan, David Ingram, and Arthur R. Smith, C. V.Kelly and Y. Ijiri, J of Appl. Phys., 93, 5274(2003).

[7] T. Dietl, H. Ohno, F. Matsukura, J. Cibert, D. Ferrand, Science **287**, 1019 (2000).

[8] M. E. Overberg, et al., Appl. Phys. Lett. 79, 1312 (2001).

[9] G. Kreiner, and H. Jacobs, J. Alloys and compounds **183**, 345 (1992).

[10] K. Suzuki, T. Kaneko, H. Yoshida, Y. Obi, H. Fujimori, H. Morita, J. Alloys and Compounds **306**, 66 (2000).

[11] A. Leineweber, R. Niewa, H. Jacobs, and W. Kockelmann, J. Materials Chemistry **10:(12)**, 2827 (2000).

[12] W.J. Takei, R. R. Heikes, and G. Shirane, Phys. Rev. **125**, 1893 (1962).

[13] B. R. Sahu and Leonard Kleinman, Phys. Rev. B**68**,113101(2003).

[14] Walter R. L. Lambrecht, M. Prikhodko, and M.S. Miao, Phys. Rev. B**68**, 174411 (2003).

[15] H.Q. Yang, H. Al-Brithen, A.R. Smith, E. Trifan, and D. C. Ingram, J.Appl. Phys. **91**, 1053 (2002).

[16] H.Q. Yang, H. Al-Brithen, A.R. Smith, J. A. Borchers, R. L. Cappelletti, M. D. Vaudin, Appl. Phys. Lett. **78**, 3860 (2001).

[17] H.Q. Yang, A.R. Smith, M. Prikhodko, W.R.L. Lambrecht, Phys. Rev. Lett. **89**, 226101 (2002).

[18] Inorganic Index to Power Diffraction File (Joint Committee on Powder Diffraction Standards, International Center for Powder Diffraction Data, Swarthmore, PA, 1997): MgO (Card No. 04-0820).

[19] H.Q. Yang and A. R. Smith, unpublished.

FIGURES

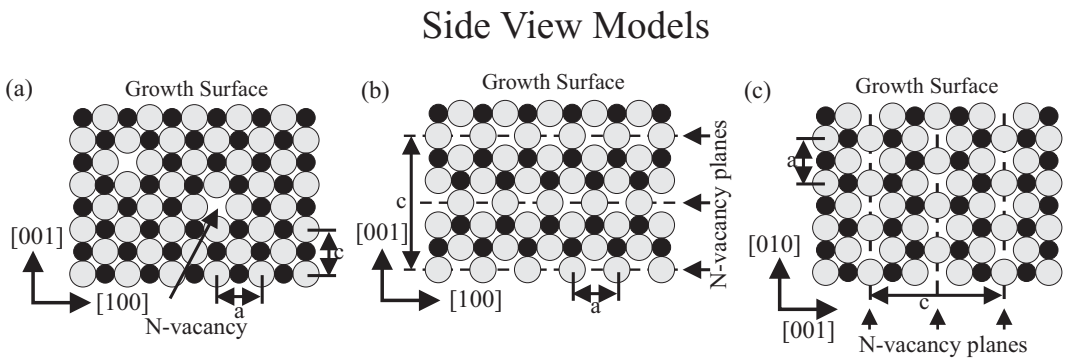

FIG. 1. Side views of schematic model structures of the different phases and orientations. Black circles are N atoms, gray circles are Mn atoms. (a) θ-phase, (b) $\eta_{\perp}$-phase, (c) $\eta_{||}$-phase.

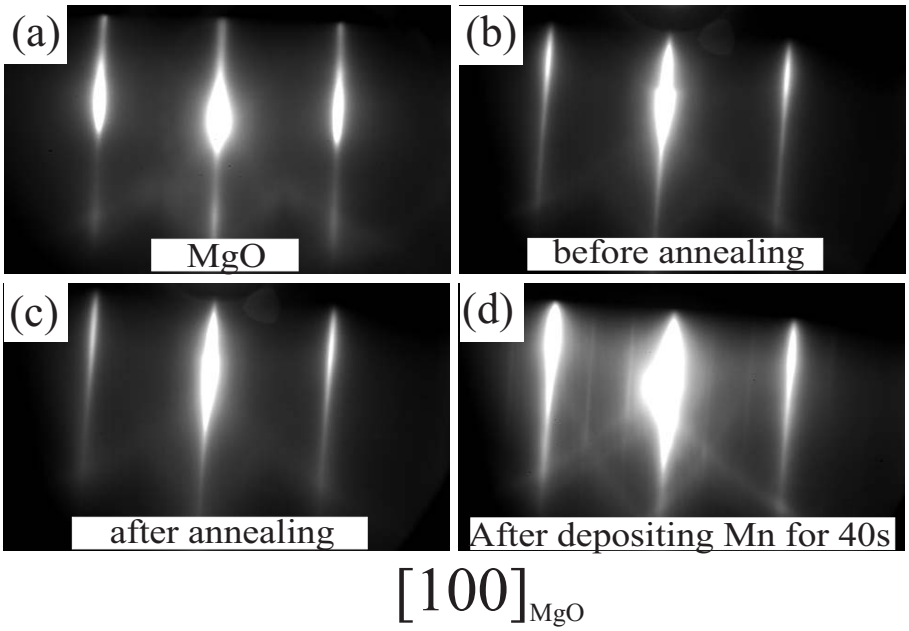

FIG. 2. RHEED patterns of θ-MnN growth and annealing sequence:(a) substrate MgO(001) along [100]; (b) θ-MnN (001) grown at 450°C along [100]; (c) after annealing at 550°C; (d) after annealing and exposure to Mn flux = 7.3×10^{13} $cm^{-2}s^{-1}$ for 40s at 550°C.

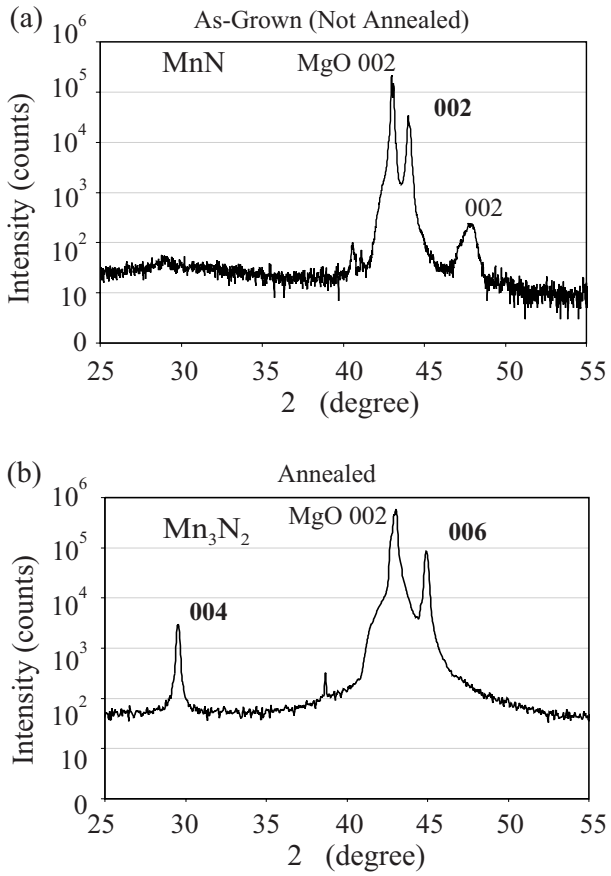

FIG. 3. XRD spectra of θ-MnN (as-grown) and after annealing, showing conversion to η-Mn_3N_2.

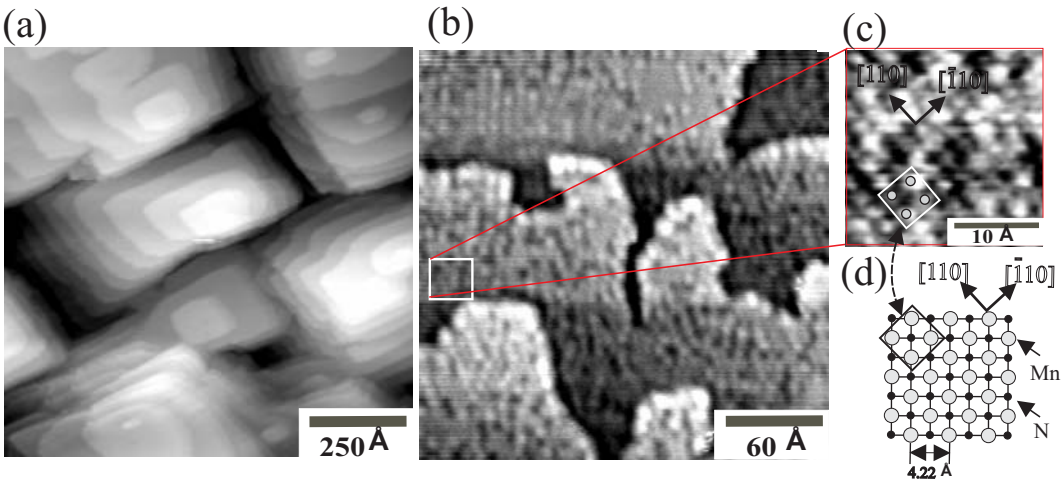

FIG. 4. STM images of θ-MnN (001) are shown. (a) STM image of 900Å $\times$ 900Å was acquired at a sample bias of 1.2 V and a tunneling current of 0.1 nA. (b) 200Å $\times$ 200Å STM image at bias voltage 0.3 V, tunneling current 0.8 nA. A local background subtraction was applied to enable viewing of all terraces; (c) Atomic resolution image of size of 25Å $\times$ 25Å, which corresponds to the small box region in (b). The sample bias is 0.1 V, tunneling current is 1.8 nA. It shows a surface with a 1$\times$1 periodicity; (d) θ-MnN (001) surface model.

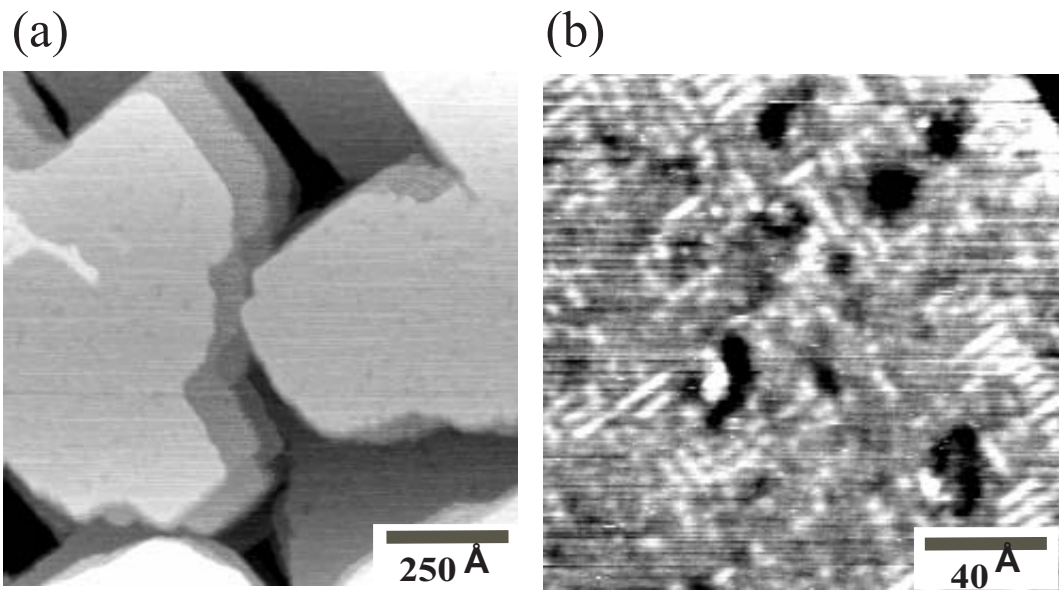

FIG. 5. STM images of surface which has transformed to η-Mn_3N_2 phase by annealing. (a) STM image of 900Å $\times$ 900Å of was acquired at a sample bias of 0.033 V and a tunneling current of 0.1 nA. (b) 150Å $\times$ 150Å STM image at bias voltage 0.093 V, tunneling current 0.1nA.

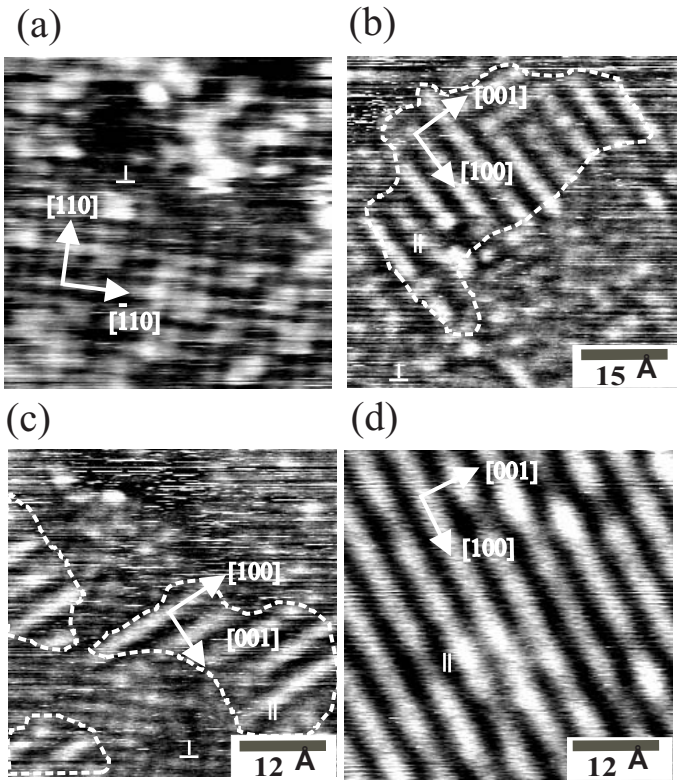

FIG. 6. (a)-(c) are three zoom-in STM images of the terrace region shown in Fig. 5(b). The sample biases of STM images in Figs. 6(a),(b) and (c) are 0.083 V, 0.053 V, and 0.031 V, respectively; the tunneling currents are all 0.1 nA. Fig. 6(d) is a STM image of $\eta_{||}$ (010) with size of 50Å $\times$ 50Å acquired at sample bias voltage of -0.4V and tunneling current of 0.4 nA.

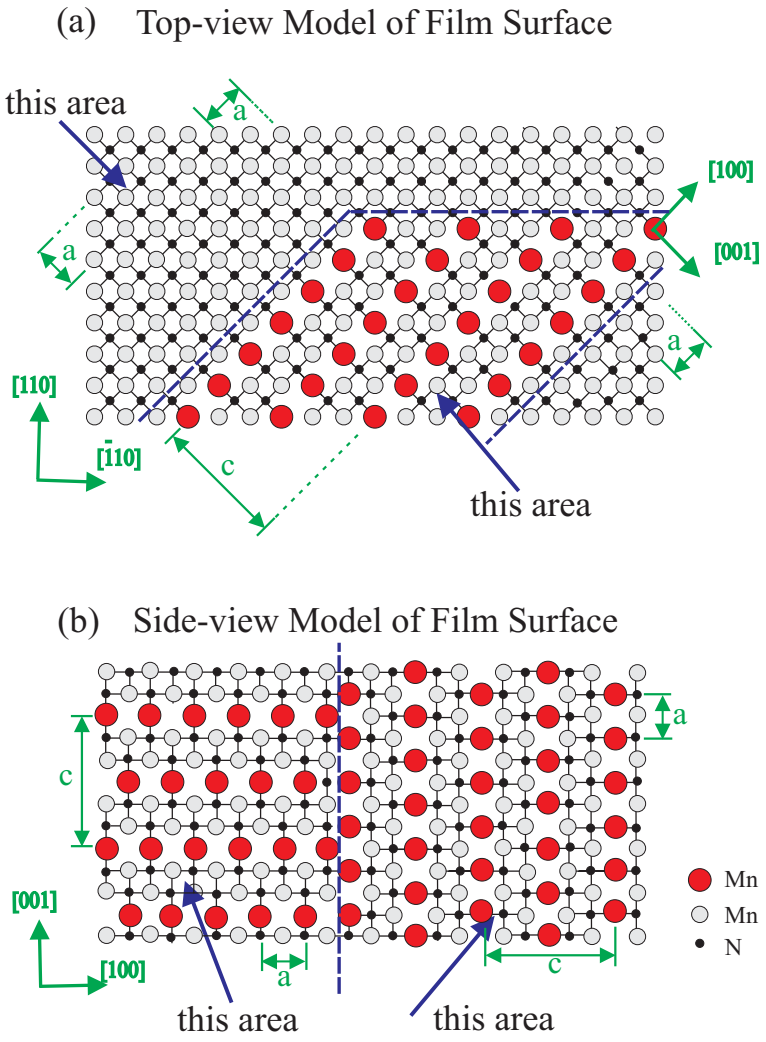

FIG. 7. Top-view and side-view schematic models of the annealed sample which has transformed from θ-MnN to η-Mn_3N_2 having 3 different orientations; 2 orientations are shown in the model. The 3rd orientation would have the $\eta_{||}$ rows at 90° compared to those shown in (a).